WIND ENERGY
Wind Energ. 2016; **00**:1–15
DOI: 10.1002/we

RESEARCH ARTICLE

Load Reduction on a Clipper Liberty Wind Turbine with Linear Parameter-Varying Individual Blade-Pitch Control

Daniel Ossmann[1], Julian Theis[2], and Peter Seiler[1]

[1] Aerospace Engineering and Mechanics, University of Minnesota, Minneapolis, MN, USA
[2] Institute of Control Systems, Hamburg University of Technology, Hamburg, Germany

ABSTRACT

The increasing size of modern wind turbines also increases the structural loads caused by effects such as turbulence or asymmetries in the inflowing wind field. Consequently, the use of advanced control algorithms for active load reduction has become a relevant part of current wind turbine control systems. In this article, an individual blade-pitch control law is designed using multivariable linear parameter-varying control techniques. It reduces the structural loads both on the rotating and non-rotating parts of the turbine. Classical individual blade-pitch control strategies rely on single control loops with low bandwidth. The proposed approach makes it possible to use a higher bandwidth since it accounts for coupling at higher frequencies. A controller is designed for the utility-scale 2.5 MW Liberty research turbine operated by the University of Minnesota. Stability and performance are verified using the high-fidelity nonlinear simulation and baseline controllers that were directly obtained from the manufacturer. Copyright © 2016 John Wiley & Sons, Ltd.

KEYWORDS

wind turbine control; load reduction; robust control

Correspondence

University of Minnesota 110 Union St SE, Minneapolis, MN 55455. E-mail: dossmann@umn.edu

Received . . .

1. INTRODUCTION

The size of modern wind turbines has been increasing over the last several years in order to lift wind turbines to a higher power production level and this trend is expected to continue. Upscaling goes hand in hand with an increase in structural flexibility and as a consequence also increases the loads on the rotating and non-rotating parts of the turbine. These loads are caused by effects such as wind shear, tower shadow, and turbulence. They can have significant impacts on the life cycle of the turbine. The demand for sophisticated control algorithms to actively mitigate these additional loads has sparked an increased industrial and academic interest. In [1], a comprehensive overview of possible load mitigation control techniques is provided, ranging from filters to damp resonances on the tower bending and the drive-train shaft torsion load to measured tower acceleration feedback via collective blade pitch that helps to suppress tower fore-aft loads. Modern wind turbines further offer the possibility to pitch each blade individually. Individual blade pitch can effectively reduce the blade's out-of-plane loads but requires additional load measurements and individual actuators on each blade [2].

A wind turbine's dynamical properties depend on the rotary hub position, making it a periodic dynamic system. Standard control approaches are thus not directly applicable. The multi blade coordinate (MBC) transformation, originally developed in the helicopter literature [3, 4], has been used in wind turbine control to overcome this issue. It projects rotating quantities onto non-rotating coordinates and facilitates control design. In fact, most individual blade-pitch controllers implemented on industrial turbines make use of MBC-transformed out-of-plane blade load signals that are a combination of edgewise and flapwise blade loads [5]. These signals are commonly processed by two single-input-single-output (SISO) integral or proportional-integral feedback controllers in order to suppress low frequency components of the loads [1, 6]. The actual blade pitch commands are then generated by inverse MBC transformation. Individual pitch commands that are calculated from the MBC transformation do not influence the collective load of the turbine. This is an important fact, as the individual

blade-pitch control algorithm should not change the thrust and the torque of the turbine in order to maintain the power output at its desired level.

Sophisticated, model-based state-space control approaches also became possible by transforming the whole periodic system into the non-rotating frame [7]. Multivariable control designs were investigated in [2] based on a linear quadratic regulator and in [8, 9] based on H_∞-norm optimal control. Adaptive control techniques for individual blade-pitch control are presented in [10]. Periodic control for load reduction using individual blade-pitch control was developed and tested in [11]. These controllers aimed at the once-per-revolution (1P) blade loads and were shown to yield similar results as the classical two-SISO-loops control strategy. A direct extension of this control strategy to target loads at higher frequencies is addressed in [12, 13] additionally using complex, higher-order transformations of the sensor data. Successful field test results of such controllers for two and three bladed turbines is presented in [14]. However, in this case, a linear analysis of the closed loop model to verify robustness and performance is not straightforward anymore. Further, it also requires several design steps instead of a single one. This is also true for the feedforward filters added in each of the two SISO loops to cope with the 3P loads on the nacelle proposed in [15]. The feedforward filters are designed using a constrained numerical optimizations technique. Due to these reasons, the classical two-SISO-loops control strategy serves for comparison in this article. The reduction of higher frequency loads was also achieved in [16, 17] by employing additional trailing edge flaps and in [18] by using additional flow measurement sensors. The disturbance accommodation techniques that are presented in [19] also achieve a small amount of load reduction for higher frequency loads.

The contribution of this article is an individual blade-pitch control design approach that can mitigate both dominant blade and nacelle loads in the turbines operational region 3. The presented approach allows targeting of loads at higher frequencies and thereby extends linear model-based approaches available in the literature. This is achieved through a multivariable design that explicitly accounts for dynamic couplings which are neglected by individual blade pitch controllers commonly used in industry. The couplings become more pronounced at higher frequencies and also strongly dependent on the pitch angle of the blades and hence on the effective wind speed. This dependence on an external parameter (wind speed) motivates the use of linear parameter-varying (LPV) control techniques [20]. The result is a controller that itself depends on the current wind speed and therefore adapts to the varying dynamics of the wind turbine. The controller is applied to the high fidelity model of the Clipper Liberty C96 research turbine operated by the University of Minnesota. The simulation model as well as the baseline controller that is used for comparison are directly obtained from the manufacturer of the wind turbine.

2. MULTI BLADE COORDINATE TRANSFORMATION

The MBC transformation is used to transform quantities from the rotating frame to the non-rotating (or fixed) frame. For example, the three out-of-plane degrees of freedom of the individual blades can be transformed to the fixed frame. Doing so results in a collective degree of freedom, in which all blades move synchronously fore and aft, and two asymmetric degrees of freedom, in which the blades move asymmetrically fore and aft [2, 5]. For a better understanding of the MBC transformation, a short review is given in this section. A detailed derivation can be found, e. g., in [7]. The transformation matrix from the rotary frame to the fixed frame is defined by

$$T(\phi) = \frac{2}{3}\begin{bmatrix} 1/2 & 1/2 & 1/2 \\ \cos(\phi) & \cos(\phi+\frac{2}{3}\pi) & \cos(\phi+\frac{4}{3}\pi) \\ \sin(\phi) & \sin(\phi+\frac{2}{3}\pi) & \sin(\phi+\frac{4}{3}\pi) \end{bmatrix}, \tag{1}$$

where ϕ is the rotary position of the first blade. The out-of-plane vector of loads $M = \begin{bmatrix} M_1 & M_2 & M_3 \end{bmatrix}^T$, measured on the three blades, can be transformed with (1) to the non-rotating frame. This results in one symmetric and two asymmetric loads [5]. The symmetric load is strongly connected to the thrust of the turbine, which is a byproduct of the moment (and power) generation. It can be effectively controlled via collective blade pitch. Individual blade pitch, on the other hand, can be efficiently used to mitigate the two asymmetric loads that appear as a cyclic pitching moment $M_{\cos}$ and a cyclic yawing moment $M_{\sin}$ on the nacelle in the fixed frame. These cyclic moments are expressed in terms of the individual blade moments as

$$\begin{bmatrix} M_{\cos} \\ M_{\sin} \end{bmatrix} = \frac{2}{3} V^T(\phi) \begin{bmatrix} M_1 \\ M_2 \\ M_3 \end{bmatrix}, \tag{2}$$

where the shorthand notation

$$V^T(\phi) = \begin{bmatrix} \cos(\phi) & \cos(\phi+\frac{2}{3}\pi) & \cos(\phi+\frac{4}{3}\pi) \\ \sin(\phi) & \sin(\phi+\frac{2}{3}\pi) & \sin(\phi+\frac{4}{3}\pi) \end{bmatrix} \tag{3}$$

Wind Energ. 2016; **00**:1–15 © 2016 John Wiley & Sons, Ltd.
DOI: 10.1002/we
Prepared using weauth.cls

was used for the last two rows of the matrix in (1). Reducing these loads is the focus of the present article. The inverse MBC transformation is given by

$$T^{-1}(\phi) = \begin{bmatrix} 1 & \cos(\phi) & \sin(\phi) \\ 1 & \cos(\phi + \frac{2}{3}\pi) & \sin(\phi + \frac{2}{3}\pi) \\ 1 & \cos(\phi + \frac{4}{3}\pi) & \sin(\phi + \frac{4}{3}\pi) \end{bmatrix}. \tag{4}$$

This transformation is required for the implementation of an individual blade-pitch controller, designed in the MBC-transformed reference frame [2]. The two cyclic control signals $\beta_{\cos}$ and $\beta_{\sin}$, generated by the controller, need to be transformed back into three blade pitch angles using the second and third column of (4). This again is more conveniently expressed as

$$\begin{bmatrix} \beta_1 \\ \beta_2 \\ \beta_3 \end{bmatrix} = V(\phi) \begin{bmatrix} \beta_{\cos} \\ \beta_{\sin} \end{bmatrix}. \tag{5}$$

The complete architecture for region 3 control is shown in Figure 1. This architecture includes the baseline controller (directly obtained from Clipper) along with the proposed individual blade-pitch controller for load reduction. The baseline controller maintains rated rotor speed via collective blade pitch β_{col}. The collective blade pitch command is calculated through proportional-integral control from measured rotational speed ω and its rated value ω_{rated}. The proposed individual blade-pitch controller controller maps the out-of-plane bending moments M to cyclic moments via the MBC. The moments M are generated using the measured flapwise and edgewise blade root bending moments. The individual blade-pitch controller (detailed in Section 4) computes cyclic blade pitch commands. The controller is scheduled by the collective blade pitch angle which provides an estimate of the wind speed. Finally the cyclic blade pitch commands are mapped back to the individual blade pitch commands β_{ind} via the inverse MBC and added to the collective blade pitch. The resulting values, β_{ref}, are sent to the blade pitch actuators.

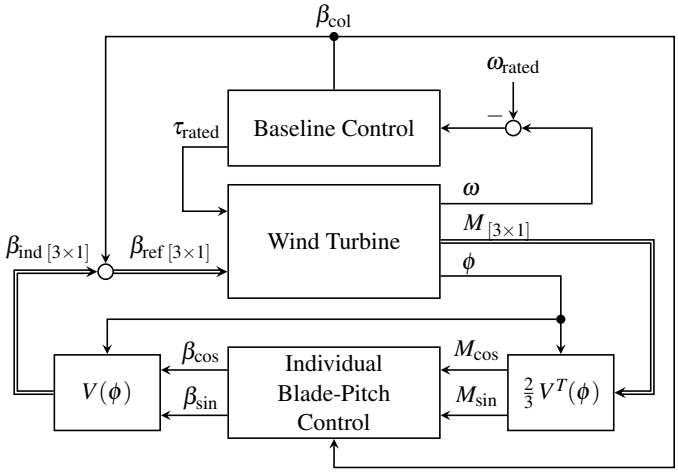

Figure 1. Control architecture for individual blade-pitch control.

3. CLIPPER LIBERTY WIND TURBINE

The wind turbine considered in this article is the utility-scale three-bladed Clipper Liberty 2.5 MW research turbine of the EOLOS Wind Energy Research Consortium located at the UMore Park in Rosemount, MN, and shown in Figure 2. It has a hub-height of 80 m and a rotor diameter of 96 m. It is common to classify the operating range into standstill (region 1), variable speed (region 2), and constant speed (region 3). The turbine's cut-in wind speed is 3 m/s, from which a $k\omega^2$ feedback law is used to control the generator torque. The range from 8 to 12 m/s is used to transition between the control laws of region 2 and region 3 and is referred to as region 2.5. The rated region 3 operation starts at about 12 m/s. The turbine cuts out at a wind speed of 25 m/s.

Figure 2. University of Minnesota's research turbine [21].

3.1. Nonlinear Model

The industrial high-fidelity nonlinear simulation model and baseline control laws used in this article were obtained directly from Clipper, the manufacturer of the Liberty Wind Turbine. While the precise details are proprietary, using this model of a utility-scale turbine and its baseline controller provides the great opportunity to assess the proposed control design in a realistic environment. The model includes a detailed structural dynamics model of the turbine with various degrees of freedom, steady aerodynamics, and linear first order models for actuators and sensors. The baseline control law for the different wind regimes includes the $k\omega^2$ feedback, the gain-scheduled collective pitch controller, transition functions, and also protection capabilities that reduce the torque and power overshoots in region 3 in case of turbulence. The model is simulated in the Fatigue, Aerodynamics, Structures, and Turbulence (FAST) software [22].

3.2. Linear Parameter-Varying Model

The FAST code provides algorithms to trim the model around a defined operating point and to derive linearized models for different rotary positions [22]. In this way, a periodic state space model in a gridded format is available. The model is of 17^{th} order and includes the rotary shaft velocity, four states to describe the tower fore-aft and side-to-side flexibility, as well as six states to describe the first flapwise bending and six states to describe the first edgewise bending of the blades in the rotary frame.

The MBC transformation can be applied not only to signals but also allows the conversion of a periodic state space model from a rotating into a non-rotating coordinate system. The derivation of the transformation can be found in detail in [7, 23]. States that represent the flapwise and edgewise degrees of freedom in the rotating frame are transformed to symmetric and asymmetric states in the fixed frame. These states are also referred to as collective and cyclic states [5]. The transformed system in the fixed frame is still periodic, but analyses have shown that it can be approximated very accurately by an LTI model that is obtained from averaging over the rotary position [7]. Such a model serves as the design model for the individual blade-pitch controller in this article. Its inputs are the cyclic pitch commands $\beta_{\cos}$ and $\beta_{\sin}$ as defined in (5) and its outputs are the cyclic moments $M_{\cos}$ and $M_{\sin}$ as defined in (2).

Having dealt with the periodicity of the system by applying the MBC transformation, it remains to address the variation of the dynamics for different wind speeds. The framework of linear parameter-varying (LPV) systems [20, 24] is a natural choice for this. LPV systems are dynamic systems whose state space representations depend continuously on a measurable time-varying external scheduling parameter $\rho(t)$ that is confined to a compact set and whose rate of variation is bounded. For the wind turbine, a natural scheduling parameter is the effective wind speed v. The wind speed can be measured using LIDAR technology as described e. g. in [25, 26]. To avoid this additional measurement for the present design, the scheduling approach described in [27, 28] is used. In region 3, the collective blade pitch is set by the baseline controller according to the wind speed. Thus, the baseline controller itself actually provides an estimate of the wind speed via the commanded collective blade pitch angle. The effective wind speed for scheduling is consequently calculated from this command through low-pass filtering and scaling and no additional sensors are required.

The admissible range for the wind speed is $v \in [12, 25]$ m/s. Bounds on the rate of variation are selected as ± 1 m/s^2. An LPV model for the wind turbine then is of the form

$$G_v\colon \begin{cases} \dot{x}(t) = A(v(t))\, x(t) + B(v(t))\, u(t) \\ y(t) = C(v(t))\, x(t) + D(v(t))\, u(t)\ . \end{cases} \tag{6}$$

Wind Energ. 2016; **00**:1–15 © 2016 John Wiley & Sons, Ltd.
DOI: 10.1002/we
Prepared using weauth.cls

Such a model can be obtained by applying the previously described procedure (linearization, MBC-transformation, and averaging) for different wind speeds along the baseline controller scheduling trajectory, defined by generator torque and blade pitch angle. Doing so yields a set of LTI models that together form a grid representation of the LPV system (6). Using four different wind speeds of 12 m/s, 16 m/s, 20 m/s, and 25 m/s yields a sufficiently dense grid and linear interpolation is then used to recover models that are between two grid points. Such a representation is not only efficient in terms of computational storage requirements but also immediately relates to intuition about linear systems. Evaluated pointwise in the parameter domain, the model recovers the LTI system that would have been obtained from linearization at that particular wind speed.

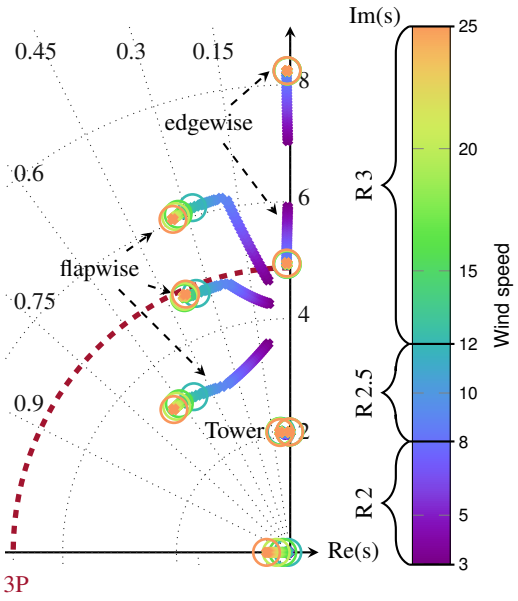

(a) Pole migration for variation in the wind speed.

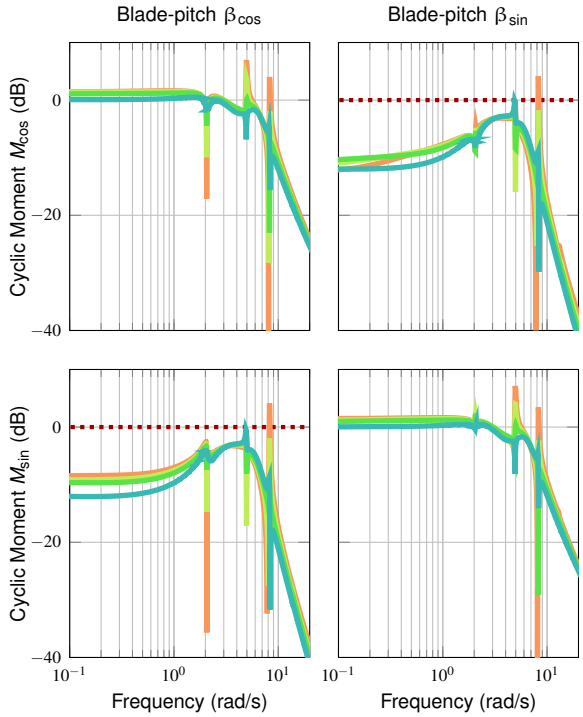

(b) Normalized frequency responses from cyclic pitch commands to cyclic moments for fixed wind speeds of 12 m/s (—), 16 m/s (—), 20 m/s (—), and 25 m/s (—).

Figure 3. Linearized, MBC-transformed and averaged models of the wind turbine.

Figure 3a depicts the poles of the resulting LTI models in dependence on the wind speed and highlights the four models that are used to form the LPV system. The pole near the origin corresponds to the rotary velocity of the turbine and almost acts as a pure integrator. The tower's first side-to-side and fore-aft modes at around 2 rad/s show low damping but remain almost constant over the wind speed. The flapwise modes increase in frequency in the region 2 and 2.5 operation. After the rated rotation speed of the turbine is reached, the damping of these modes increases with increasing wind speed while the frequency remains unchanged. The red line in the figure represents the 3P ($\approx$4.8 rad/s) frequency of the turbine in region 3. The term "P" refers to *per revolution* and indicates multiples of the rotational frequency of the turbine. One of the flapwise modes and one of the edgewise modes can be seen to approach the 3P frequency. An overlapping of the turbine modes with these frequencies potentially causes problems, as normal operation of the turbine excites dynamics at these frequencies. The flapwise mode that approaches the 3P frequency is considered safe, as it is rather well damped. The edgewise mode, on the other hand, is likely to cause unwanted effects in region 3, due to its poor damping. The third edgewise mode is located around 13 rad/s and is not shown in the figure. It should also be noted that the pure integrator pole that corresponds to the rotor position is removed from the model and not shown since it is of no interest for the control problem.

Figure 3b shows the frequency response from cyclic blade pitch commands to cyclic moments for the four LTI models that are used to form the LPV model. They are normalized by the DC-gains of the diagonal elements at 12 m/s wind speed. Consequently, the diagonal elements have a gain close to unity, with noticeable resonances at 1P ($\approx$1.6 rad/s) and 3P ($\approx$4.8 rad/s), as well as 8 rad/s, which is the frequency of the collective edgewise mode. These resonances clearly depend on the wind speed and become more pronounced at higher speeds.

That is, while the corresponding poles remain almost unchanged throughout region 3 as a consequence of the constant rotor speed, the dynamic properties nevertheless vary considerably. Specifically, the contribution of the two edgewise modes to the cyclic moments increases with higher wind speeds as a consequence of the larger collective blade pitch angle. The off-diagonal elements have magnitude values of around $-10\,\mathrm{dB}$ in the low frequency range but the coupling increases with magnitudes comparable to, and even above, those of the diagonal elements at frequencies above 1P. Again, the resonances depend on the wind speed. These observations are the main motivation for the use of multivariable LPV control to achieve load reduction with higher bandwidth.

4. LINEAR PARAMETER-VARYING CONTROL DESIGN

The control objectives need to be formulated in terms of the fixed frame dynamics that are represented by the MBC-transformed and averaged model. One objective is to reduce the 1P load in the rotating frame. However, the dynamic model used for control design is formulated in the fixed frame via the MBC transformation as described in Section 3.2. The 1P load in the rotating frame mainly translates to a dominant constant (0P) load in the fixed frame with smaller components at the 3P frequency. Thus load reduction at zero frequency in the fixed frame will significantly reduce the 1P load in the rotating frame. The classical two-integral-loops approach makes use of this fact. The controller designed in this article will additionally achieve load reduction at 3P in the fixed frame, mainly resulting from the 2P and 4P frequency in the rotary frame. Increasing the bandwidth to achieve 3P reduction in the fixed frame requires a multivariable design to account for the dynamic coupling from the two cyclic pitch inputs to the two cyclic loads (Figure 3b).

H_∞ control is particularly useful for this task since it allows to directly "shape" the closed-loop frequency response to meet these requirements. A direct extension to LPV systems, referred to as induced L_2-norm control, is also readily available [29]. One key feature of the approach is that linear intuition is to a certain extend preserved. The induced L_2-norm of an LPV system H_ρ from input d to output e is defined as

$$\|H_\rho\|_\infty = \sup_{\substack{d\in L_2\setminus\{0\}\\ \rho\in\mathscr{A}}} \frac{\|e\|_2}{\|d\|_2} \tag{7}$$

The induced L_2-norm measures the maximum gain of H_ρ, i. e., the largest amplification of L_2 input signals over all frequencies, input/output directions, and admissible parameter trajectories. The control problem is formulated as the closed-loop interconnection shown in Figure 4a and described by the input-output map

$$\begin{bmatrix} e_1 \\ e_2 \end{bmatrix} = \begin{bmatrix} W_u & \\ & W_e \end{bmatrix} \begin{bmatrix} -T_i & K_\rho S_\mathrm{o} \\ -G_\rho S_\mathrm{i} & S_\mathrm{o} \end{bmatrix} \begin{bmatrix} W_1 & \\ & W_2 \end{bmatrix} \begin{bmatrix} d_1 \\ d_2 \end{bmatrix}. \tag{8}$$

The LPV plant model is denoted G_ρ, K_ρ is the LPV controller, $S_\mathrm{o} = (I + G_\rho K_\rho)^{-1}$ is the output sensitivity function, $S_\mathrm{i} = (I + K_\rho G_\rho)^{-1}$ is the input sensitivity function, and $T_\mathrm{i} = K_\rho G_\rho (I + K_\rho G_\rho)^{-1}$ is the complementary input sensitivity function [30]. Further, $K_\rho S_\mathrm{o}$ is called control sensitivity and $G_\rho S_\mathrm{i}$ is called disturbance sensitivity. Performance is measured by the induced L_2-norm from $d = \left[\begin{smallmatrix} d_1 \\ d_2 \end{smallmatrix}\right]$ to $e = \left[\begin{smallmatrix} e_1 \\ e_2 \end{smallmatrix}\right]$ and the weights W_u, W_e, W_1, and W_2 specify how the involved sensitivity functions contribute to the performance criterion. The weights for the present design are

$$W_u = I_2\, 500\, \frac{s+3.464}{s+3464}, \qquad W_e = I_2\, 0.1\, \frac{s+3}{s+0.03}\, \frac{s^2+0.49s+24}{s^2+6.93s+24}, \qquad W_1 = I_2 \qquad \text{and} \qquad W_2 = I_2\, 0.1\,. \tag{9}$$

Figure 4b shows magnitude plots of the weighting filters. Their inverses dictate the shape of the sensitivity functions and their choice is discussed next.

The goal of the control design can be summarized as reducing the sensitivity to disturbances at frequencies that are relevant for loads. The setup (8) models the disturbances d_1 to occur at the plant input, i. e., as disturbances to the cyclic blade pitch angles. This is a reasonably simple model for general wind disturbances that induce an angle-of-attack at the blades and hence have a similar effect as a change in the blade pitch angle. The filter W_e is used to shape the disturbance sensitivity function $G_\rho\, S_\mathrm{i}$. With the normalized plant model as shown in Figure 3b and the input weight $W_1 = I_2$, a gain of W_e larger than 1 at a given frequency dictates a sensitivity reduction at that frequency and hence improves disturbance rejection. Since the 0P load in the fixed frame needs to be suppressed similar to the classical individual blade-pitch control strategy, W_e is selected as a diagonal transfer function matrix with a high gain in the low-frequency range up to 0.3 rad/s. An additional penalty is added in the vicinity of the 3P frequency of about $4.8\,\mathrm{rad/s}$ by multiplying the low frequency weight with an inverse notch filter, tuned to that frequency. This modification expresses the requirement to specifically decrease the sensitivity at that frequency and hence to actively suppress the 3P loads. The complementary input sensitivity T_i describes the control effort in response to input disturbances and is a measure of robustness (see e. g. [31]). A roll-off

Wind Energ. 2016; **00**:1–15 © 2016 John Wiley & Sons, Ltd.
DOI: 10.1002/we
Prepared using weauth.cls

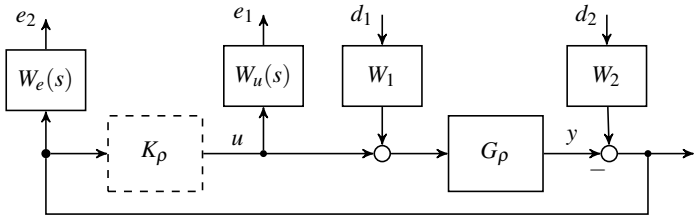

(a) Generalized plant interconnection for the individual blade-pitch H_∞ control design.

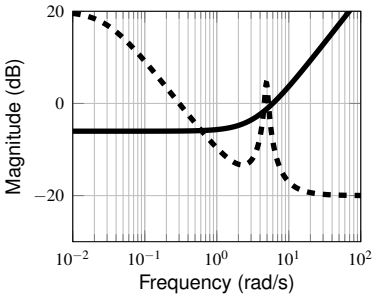

(b) Singular value plots of the selected weighting filters w_e (▪ ▪ ▪) and w_u (▬▬).

Figure 4. Formulation of the control objectives in terms of a generalized plant and weighted signals.

below the Clipper Liberty's actuator bandwidth of around 10–15 rad/s is desirable and peaks should be limited to less than 2 for reasonable robustness. Hence, W_u is selected as a diagonal transfer function matrix with a low frequency gain of 0.5, a 0 dB crossing at 6 rad/s and approximately differentiating behavior beyond 6 rad/s. A roll-off in T_i, however, does not necessarily translates to a roll-off in K. Hence, output disturbances d_2 are considered to include the control sensitivity in the problem formulation. The weight W_u then also forces the controller to roll off with 20 dB/dec beyond 6 rad/s in order to prevent high frequency control action that may result in hitting the actuators' rate limits and cause pitch actuator fatigue. The matrix W_2 is tuned to $0.1\,I_2$ in order to allow sufficient control activity magnitude. The resulting requirements on S_o from W_2 and W_e can be seen to be redundant and hence inactive. The determining factor is the requirement on $G_\rho\,S_\text{i}$ that implies a sensitivity reduction with an effective additional weight equal to the inverse plant model, see e. g. [32].

A parameter dependent dynamic controller K_ρ that minimizes an upper bound on the induced L_2-norm of the interconnection in Figure 4a and that also ensures stability of the closed loop and can be synthesized by solving a convex optimization problem [29]. Specifically, let an admissible parameter set $\mathscr{A}$ and the open loop LPV system interconnection

$$P_\rho\colon \left\{ \begin{bmatrix} \dot{x} \\ e_1 \\ e_2 \\ y \end{bmatrix} = \begin{bmatrix} A(\rho) & B_{11}(\rho) & B_{12}(\rho) & B_2(\rho) \\ C_{11}(\rho) & D_{1111}(\rho) & D_{1112}(\rho) & 0 \\ C_{12}(\rho) & D_{1121}(\rho) & D_{1122}(\rho) & I \\ C_2(\rho) & 0 & I & 0 \end{bmatrix} \begin{bmatrix} x \\ d_1 \\ d_2 \\ u \end{bmatrix} \right. \tag{10}$$

be given. The special structure in (10) is not restrictive, as it can be achieved through loop-shifting and scalings under mild conditions, see [33]. Denote $C_1^T = [C_{11}^T\ C_{12}^T]$, $B_1 = [B_{11}\ B_{12}]$, and $\left[\begin{smallmatrix} D_{111\bullet} \\ D_{112\bullet} \end{smallmatrix}\right] = \left[\begin{smallmatrix} D_{1111} & D_{1112} \\ D_{1121} & D_{1122} \end{smallmatrix}\right] = [D_{11\bullet1}\ D_{11\bullet2}]$. The controller can be constructed by closed formulae from the open loop plant matrices and the feasible values of X_ρ, Y_ρ, and γ of the optimization problem [20, 29]:

$$\min_{\gamma, X_\rho, Y_\rho} \gamma \text{ such that } \forall\, \rho \in \mathscr{A}\colon$$

$$\begin{bmatrix} X_\rho & \frac{1}{\gamma} I \\ \star & Y_\rho \end{bmatrix} \succ 0, \quad \begin{bmatrix} \Lambda_X - B_2 B_2^T & X_\rho C_{11}^T & \frac{1}{\gamma}(B_1 - B_2 D_{112\bullet}) \\ \star & -I & \frac{1}{\gamma} D_{111\bullet} \\ \star & \star & -I \end{bmatrix} \prec 0, \quad \begin{bmatrix} \Lambda_Y - C_2^T C_2 & Y_\rho B_{11} & \frac{1}{\gamma}\left(C_1^T - C_2^T D_{11\bullet2}^T\right) \\ \star & -I & \frac{1}{\gamma} D_{11\bullet1}^T \\ \star & \star & -I \end{bmatrix} \prec 0 \tag{11}$$

The expression $M \succ (\prec) 0$ denotes M is positive (negative) definite, $\Lambda_X = X_\rho\,(A - B_2 C_{12})^T + (A - B_2 C_{12})\,X_\rho - \frac{\partial X_\rho}{\partial \rho}\,\dot{\rho}$, $\Lambda_Y = Y_\rho\,(A - B_{12} C_2) + (A - B_{12} C_2)^T\,Y_\rho + \frac{\partial Y_\rho}{\partial \rho}\,\dot{\rho}$, and $\star$ denotes symmetric completion. It should be noted that the parameter rate $\dot{\rho}$ appears in the terms Λ_X and Λ_Y and that the constraints in (11) need to be satisfied for both the minimum and maximum values of the rate. In order to arrive at a tractable formulation, the positive definite matrix functions $X_\rho\colon \mathscr{A} \mapsto \mathbb{R}^{n_x \times n_x}$ and $Y_\rho\colon \mathscr{A} \mapsto \mathbb{R}^{n_x \times n_x}$ must further be formulated in terms of a predefined set of basis functions as

$$X_\rho = \sum_{i=1}^{a} f_i(\rho)\, X_i, \quad X_i \in \mathbb{R}^{n_x \times n_x} \quad \text{and} \quad Y_\rho = \sum_{i=1}^{b} g_i(\rho)\, Y_i, \quad Y_i \in \mathbb{R}^{n_x \times n_x}. \tag{12}$$

It is important to emphasize that the conditions used in the optimization problem are only sufficient and that the potential loss in performance is related to the conservatism that is introduced by restricting the search space for X_ρ

and Y_ρ. Thus, more basis functions usually increase performance. Constant basis functions for X_ρ and Y_ρ result in an infeasible optimization problem for the present design. Linearly parameter dependent basis functions yield a controller, but the performance is severely degraded when compared to a pointwise H_∞ design. Quadratic basis functions, i. e. $X_\rho = X_0 + X_1\,\rho + 0.5\,X_2\,\rho^2$ and $Y_\rho = Y_0 + Y_1\,\rho + 0.5\,Y_2\,\rho^2$, finally yield a satisfactory solution that almost completely recovers the performance of a pointwise H_∞ design. The required computational time is 10 minutes on a desktop PC using the routine `lpvsyn` of the openly available LPVTools toolbox [34, 35], that implements the convex optimization problem (11).

The LPV controller depends on the wind speed as a scheduling signal, for which a suitable surrogate is available from the collective pitch baseline controller as discussed in Section 3.2. As a consequence of using parameter dependent basis functions, the LPV controller in addition also depends on the rate of change of the wind speed, that is difficult to estimate. It is decided to neglect this rate dependence and to use the LPV controller that corresponds to zero rates. Frequency response plots of that controller at the grid points are shown in Figure 5a. It feeds back the MBC-transformed out-of-plane blade loads $M_{\cos}$ and $M_{\sin}$ to the cyclic pitch commands $\beta_{\cos}$ and $\beta_{\sin}$ and can be seen to vary substantially for different wind speeds. The decision to neglect the rate dependence is justified by the comparison in Figure 5b. The central plot in Figure 5b ($\dot\rho = 0$) corresponds to zero rate and is an excerpt of the magnitude plot from $M_{\cos}$ to β_{sin} in Figure 5a. The plot above ($\dot\rho = -1$) shows the controller evaluated at the four wind speeds with minimum rate of change and the plot below ($\dot\rho = +1$) shows the controller evaluated with maximum rate of change. The difference between these three plots is an indicator for the rate dependence of the controller. Compared to the difference between the different colors (that indicate the parameter dependence), the rate has little influence on the controller. Similar results can be obtained for the other three channels. The decision to neglect the rate dependence is further backed up by nonlinear simulation runs with and without rate scheduling, with differences in the loads of around 5% for tower side-to-side moments and about 0.5% for all other moments. The controller is implemented as a lookup table with linear interpolation for the state space matrix elements.

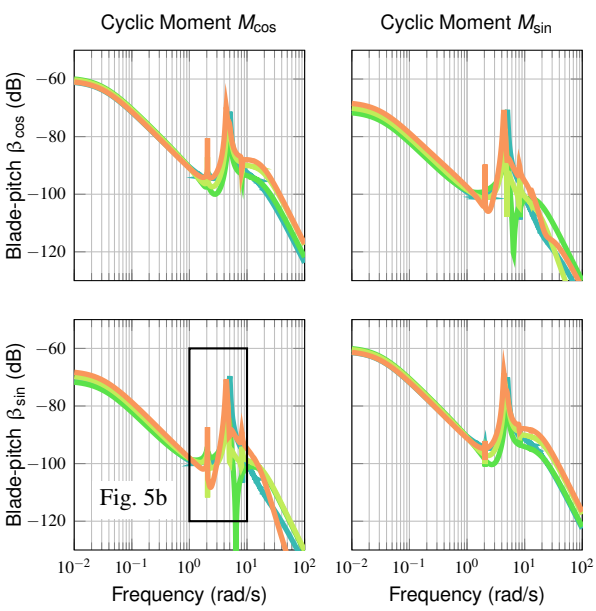

(a) Controller variation with respect to parameter.

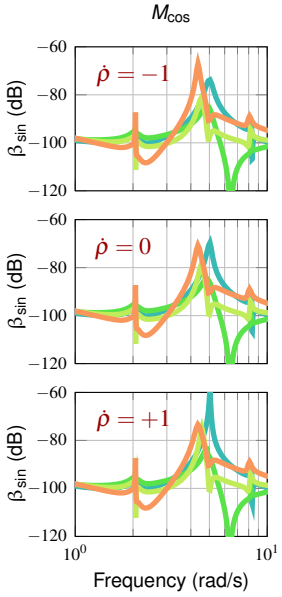

(b) Controller variation with respect to parameter and rate.

Figure 5. Frequency response of the LPV controller (cyclic moments in kNm, cyclic blade-pitch in degrees) at 12 m/s (—), 16 m/s (—), 20 m/s (—), and 25 m/s (—) fixed wind speed.

5. VERIFICATION

5.1. Frequency Responses

The controller achieves a significant reduction of the disturbance sensitivity at all grid points, as confirmed by the singular value plots in Figure 6. For low frequencies ($<0.8\,\mathrm{rad/s}$) and around 3P ($\approx 4.8\,\mathrm{rad/s}$), the magnitude of the closed loop lies clearly below the open loop plot. As an inevitable consequence of Bode's sensitivity integral [30, 36], the sensitivity is

Wind Energ. 2016; **00**:1–15 © 2016 John Wiley & Sons, Ltd.
DOI: 10.1002/we
Prepared using weauth.cls

increased at other frequencies, but the area of degradation is confined to frequencies between 1P and 3P. A tiny resonance can be observed that corresponds to the tower side-to-side mode being coupled into the response by the proposed controller. This is an undesired consequence, but the sensitivity degradation can still be characterized as well behaved with a peak of less than 6 dB. In the high frequency regime beyond 3P, open loop and closed loop are indistinguishable. This confirms low control activity at high frequencies. Figure 6 further illustrates how the disturbance sensitivity is indeed shaped by the weight W_e.

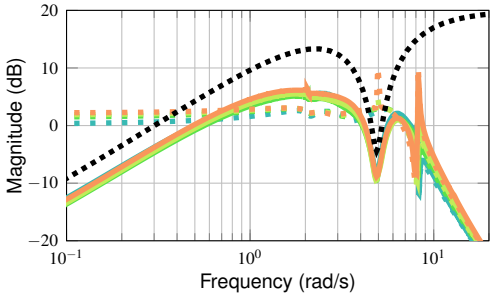

Figure 6. Decrease in disturbance sensitivity due to the proposed individual blade-pitch controller. Singular value plots of disturbance sensitivity at grid points: open loop (dashed), closed loop (solid) and scaled inverse weight γW_e^{-1} (▪▪▪▪▪)

5.2. Robustness Margins

The most common metric to quantify robustness for a control system is given by the classical gain and phase margins. The former specifies how much gain variation a single loop-transfer function can tolerate before instability occurs. The second measures the amount of phase loss that this loop can tolerate. Both margins are independent of each other. There are different specifications depending on the application field. For example, stringent certifications requirements in aerospace require at least 6 dB gain margin and 60 deg phase margin. These requirements also serve as a basis for the controller analysis in this article. While these margins are of great practical importance, they can overlook destabilizing combinations of gain and phase that independently are considered safe. It is therefore important to take into account simultaneous gain and phase variations. The corresponding metric is known as disk margin and can be calculated from $S_i - T_i$ and $S_o - T_o$, for the inputs and the outputs of the plant, respectively [37]. They are easily extended to the multivariable case, allowing for simultaneous perturbation of several loops. The multi-input-multi-output disk margin considers simultaneous perturbation of all feedback signals and is obtained by breaking all loops both at the inputs and outputs at the same time. The margins of the proposed control loop are evaluated between 12 and 25 m/s wind speed with a step size of 1 m/s and are depicted in Figure 7.

The margins vary depending on the wind speed but are satisfactory in all wind scenarios. The worst cases for all gain margins are found at maximum wind speed, where the classical gain as well as the disk margin show values of approximately 4.8 dB and the multi-input-multi-output margin a value of around 2.5 dB. This is considered to be satisfactory. The classical phase margin is around 70 deg at minimum showing a very robust behavior. To illustrate the main motivation of the LPV controller, the margins are compared to those achieved with a previous LTI design in [38]. In that paper, an H_∞ controller was designed for a fixed wind speed of 12 m/s with the same specifications as the LPV controller. Note that the design point of 12 m/s was chosen in [38] as it provided the highest worst case margins compared to other design wind speeds. Compared to the LPV controller, the H_∞ controller achieves greater robustness for its specific design condition at 12 m/s, but the margins degrade with higher wind speeds. Clearly, the LPV design resolves that issue and provides good robustness over the whole region 3. The worst case margins using the LPV controller lie clearly above the margins provided by the H_∞ controller. Thus, using an additional measurement to schedule the controller increases the augmented systems overall robustness to uncertainties.

5.3. Nonlinear Simulations

The LPV controller is validated via nonlinear simulations using the FAST model of the Liberty turbine that was described in Section 3. As pointed out before, this model is obtained directly from the manufacturer of the wind turbine and provides a realistic environment for evaluation. In the presented analysis, the first bending modes of the shaft, of the tower in side-to-side and fore-aft direction, and of the blades in edgewise and flapwise direction are included. The test scenarios include step-like responses to evaluate the steady-state behavior and turbulent wind conditions. The latter are used first to verify load mitigation at different frequencies using power spectral densities of the gathered signals, followed by a statistical analysis to quantify the load reduction capabilities of the controller.

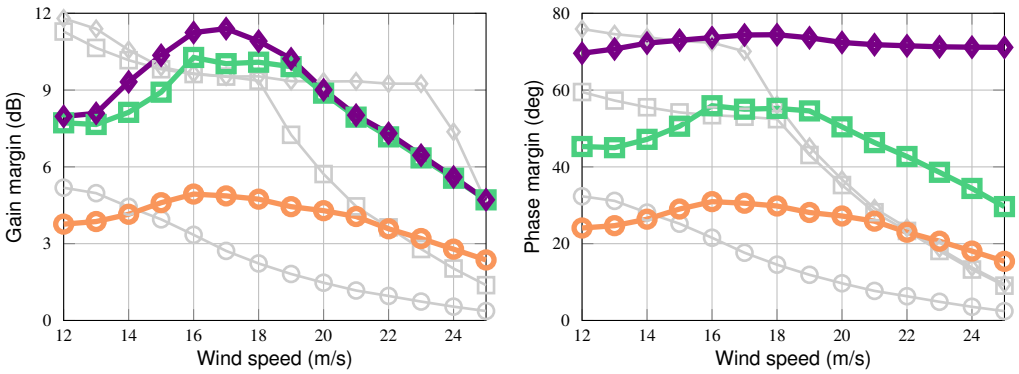

Figure 7. Classical (), disk (), and multi-input-multi-output () margins of the LPV controller over wind speed. For reference, the margins achieved with an H_∞ controller designed for 12 m/s wind speed are shown in gray.

Step-like responses

Starting at 12 m/s, the wind speed v_{hub} at hub height $h_{\text{hub}} = 80\,\text{m}$ is increased every 50 s by 2 m/s within 2 s until reaching 25 m/s. A vertical power law shear profile $v(h) = v_{\text{hub}}(h/h_{\text{hub}})^{0.14}$ is used to describe the dependence on the height h [39]. Horizontal shear is considered by increasing the wind speed linearly from right to left (looking downwind) with a difference $\Delta v = 0.12 v_{\text{hub}}$ between the left and right edge of the rotor.

Figure 8 depicts the controller input signals $M_{\cos}$ and $M_{\sin}$, the out-of-plane blade bending moment, and the resulting nacelle yawing and pitching moments measured at the bearing between tower and nacelle. The controller shifts both cyclic moments to zero mean and further clearly reduces their higher frequency (3P) content. As a result, the amplitude of the blade bending moment oscillation, which increases as a result of increasing aerodynamic forces with higher wind speeds, is clearly reduced by the controller. The average out-of-plane blade bending moment is unaffected by the proposed controller and decreases for higher wind speeds as the larger collective pitch angle directs the flapwise loads more into the rotary plane. The average nacelle yawing moment is decreased by the individual blade-pitch controller as an immediate consequence of decreasing the 1P oscillations on the blades. The remaining constant component of about $-180\,\text{kNm}$ results from the in-plane blade bending and gyroscopic effects due to the rotation causing a yaw moment on the nacelle. As these effects are not captured by the out-of-plane measurements and thus not fed back, they cannot be mitigated by the controller. The average nacelle pitching moment is decreased to higher negative values as the 1P blade loads related to wind shear in the vertical direction are reduced. The vertical wind shear actually causes a pitch-up moment in the fixed frame that opposes the gravity-induced pitch-down moment. Thus, by reducing these shear effects, the overall nacelle pitching moment is further decreased. All of these results are consistent with standard individual blade-pitch control.

In addition, the oscillatory components of the nacelle's yawing and pitching moments are also clearly reduced. Figure 9 shows the moments plotted over the rotor position for a hub-height wind speed of 25 m/s and confirms that the oscillations indeed have a dominant 3P component in the fixed frame. These oscillations are caused by higher frequency (>1P) loads on the blades and their successful reduction thus confirms that the proposed controller also performs adequately at frequencies beyond 1P. Figure 9 also shows the corresponding individual blade pitch command issued by the LPV controller. It is largely dominated by 1P action and resembles the command signal of standard individual blade-pitch controllers. Higher frequency control action has very small magnitudes and is barely visible.

Power spectral densities under turbulent wind

For a more realistic verification, turbulence needs to be considered. A wind field with at a mean hub-height wind speed of 20 m/s following the IEC-A standard, a wind speed depended turbulence intensity defined by the International Electrotechnical Commission (IEC), is chosen for this test. The wind field has been generated using the Turbsim software [40]. Due to the influence of turbulence, considering power spectral densities (PSDs) is a better choice for this analysis instead of time domain plots. Besides the baseline controller, an individual blade-pitch controller used on many modern wind turbine is used for comparison. This controller consists of two decoupled SISO integral compensators of the form $\frac{0.001}{s}$, leading to an open loop bandwidth (0 dB crossing) of around $0.25\,\text{rad/s}$. In the upper left diagram of Figure 10, the PSD of the bending moment of the first blade is depicted. The simulation results for the baseline controller without individual blade-pitch control show a dominant peak at the 1P frequency around 1.6 rad/s. Around the 2P frequency (3.2 rad/s), an increased loading is present. The integral individual blade-pitch controller is able to mitigate the 1P load very well. The LPV controller also achieves this reduction in the 1P load but additionally reduces the 2P loads on the blades. The reduction of loads at higher frequencies is again confirmed when analyzing the loads that act on the fixed

Wind Energ. 2016; **00**:1–15 © 2016 John Wiley & Sons, Ltd.
DOI: 10.1002/we
Prepared using weauth.cls

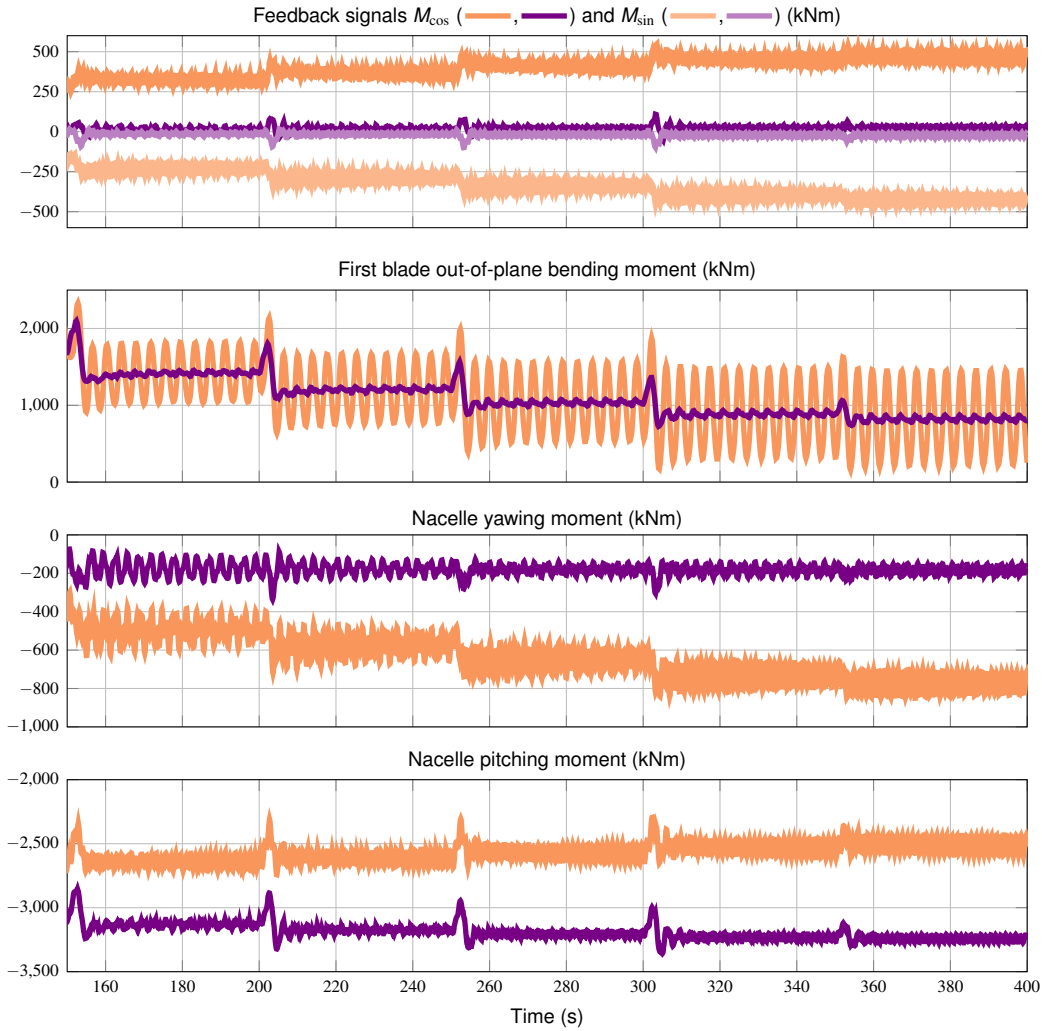

Figure 8. Time series comparison of the baseline controller ( ) and the LPV controller ( ) for step changes in wind.

frame, namely the yawing and pitching moments on the nacelle in the two diagrams on the right in Figure 10. The 1P blade loads mainly appear as a constant load in the non-rotating frame. Thus, just as the 1P load on the blades, this constant load in the non-rotating frame is mitigated well by both individual blade-pitch controllers. The 2P load on the blades produces a dominant 3P load in the fixed frame. This load is suppressed only by the LPV controller. Suppressing this load requires higher activity of the blade pitch actuation system. This is depicted in the lower left diagram of Figure 10. For low frequencies (<0.6 rad/s), all three controllers provide the same pitch action, due to the dominance of the baseline control law, commanding collective pitch. Around the 1P frequency, both individual blade-pitch controllers show an increase in control action in order to mitigate the 1P blade load. The LPV controller further shows a 2P control component with a spectrum that closely resembles the spectrum of the 2P blade loads without active control at this frequency (see the two zoomed-in plots in Figure 10). This additional control effort is required to mitigate the 2P blade loads and its magnitude relates to a classical control effort vs. performance trade-off.

Statistical load verification

To verify and quantify the load reduction capabilities, the controller is simulated under different turbulent wind conditions. The wind field files are generated using the Turbsim software [40]. The simulation time for each wind file is set to 10 minutes, ensuring that the mean hub-height wind speeds equals the defined mean value over the simulation time. The Kaiman model is selected as the turbulence spectral model. The turbulence intensity again follows the IEC-A category. Category “A” defines the highest level of turbulence intensity. Intensity levels “B” and “C” gave very similar results as the ones presented herein.

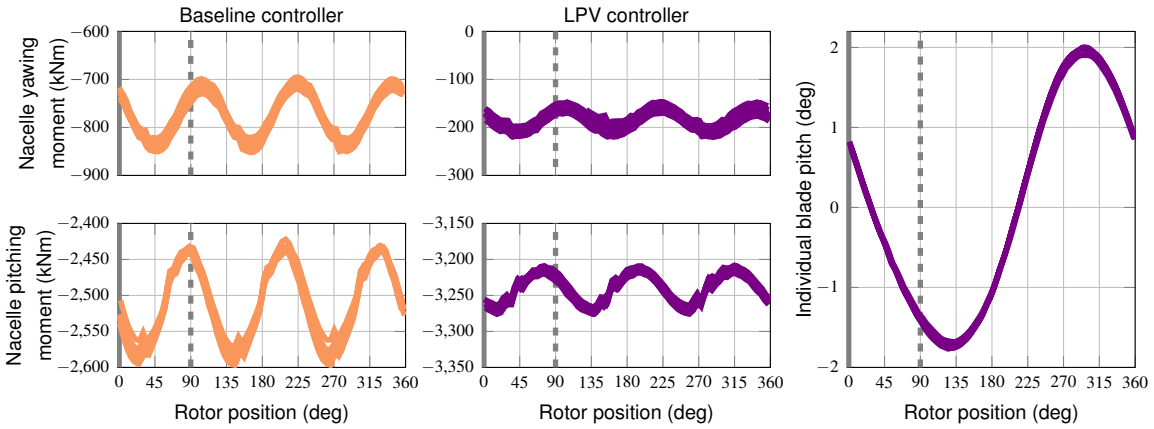

Figure 9. Blade root out-of-plane bending moment, nacelle yawing moment, and nacelle pitching moment for the baseline controller (—) and the LPV controller (—) at a wind speed of 25 m/s and corresponding individual blade pitch command. The solid line (—) represents the upright and the dashed line (- - -) the 90 deg rotor position when looking downwind.

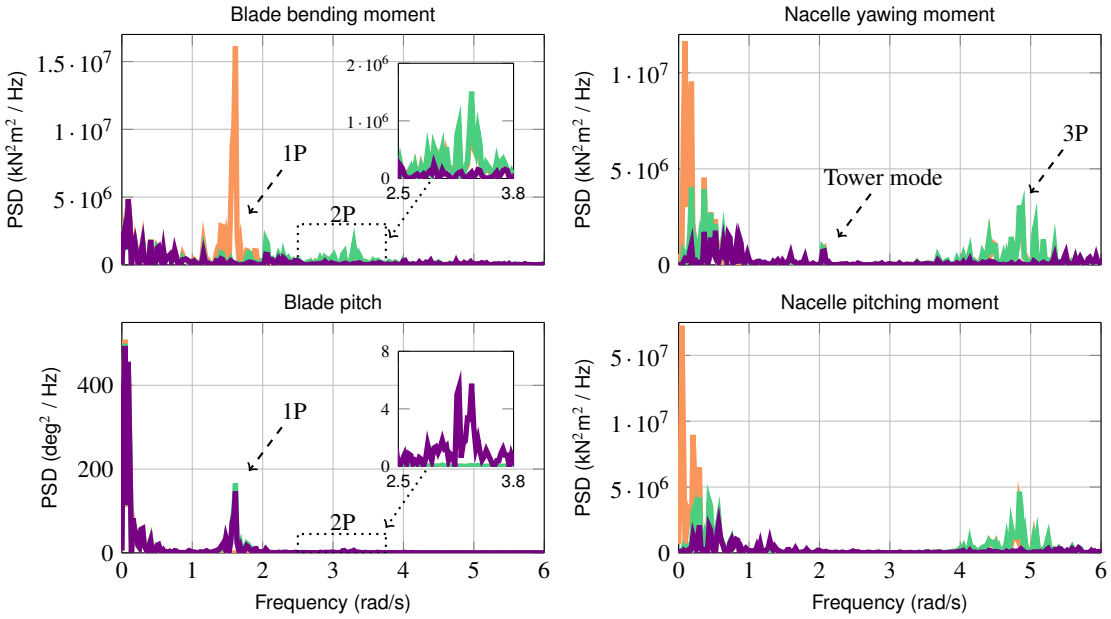

Figure 10. Power spectral densities for blade moment, nacelle yawing moment, nacelle pitching moment and blade pitch commands comparing baseline (—), two SISO integral loops (—) and LPV controller (—).

The tests were run for the whole operational region 3 of the turbine, reaching from 12 m/s to 25 m/s with 1 m/s step size. The generation of the standardized IEC wind fields makes use of the Kaiman spectra. These spectra depend on a chosen random seed [41]. Thus, for each wind speed 10 wind files based on different randoms seeds were generated. To be able to compare the results, the same tests were run with the baseline controller and the baseline controller augmented with the classical individual blade-pitch controller. Considering 3 turbulence categories, 14 wind velocities, 10 random seeds, and 3 controllers resulted in a simulation campaign of 1260 runs and required approximately 60 hours of calculation time. It is worth noting that the process was fully automated. From the gathered simulation data, the damage equivalent loads (DELs) are calculated using the software tool MCrunch [41]. DELs simplify the process of producing fatigue test loads from a design load spectrum. They can be calculated without specific knowledge of the blade structure or geometry. The main inputs are the time signal and the properties of the material (S-N slope) [42]. The DELs represent a measure of equivalent fatigue damage caused by each load and take into account material properties [2]. In this work, S-N slopes of 4 for the tower and the nacelle and 10 for the blades are used, representative for typical steel and composite materials.

Wind Energ. 2016; **00**:1–15 © 2016 John Wiley & Sons, Ltd.
DOI: 10.1002/we
Prepared using weauth.cls

The target damage equivalent loads of the control design are the loads on the blades and the nacelle. Additionally, the tower loads and the shaft loads are presented. Figure 11 shows a statistical evaluation of the generated loads. Box-plots of the different loads at 12, 18, and 25 m/s wind speed are shown for the three controllers. All box plots are normalized with respect to the maximum loads that occur with the baseline controller. The end of the antennas of each box is defined by the lowest data point still within 1.5 interquartile range of the lower quartile and the highest data point still within 1.5 interquartile range of the upper quartile. The circles indicate the remaining data point outside of these ranges. The black horizontal lines represent the median value. Both, the two-loop-integral and the LPV controller are able to reduce the blades' (out-of-plane) bending DELs at all wind speeds, but the LPV controller achieves higher reduction, specially at increased wind speeds. Note that in Figure 11 only the results for the first blade are presented as the results for the other two blades are very similar. The main advantage of the LPV controller becomes clear when the pitching and yawing loads on the nacelle are considered. Due to the control activity around the 3P frequency, the mean values of these loads can be reduced by about 25 % depending on the mean wind speed. The classical individual blade-pitch controller lets these loads unchanged. Load reduction is also effective on the shaft, where the mean value of the bending moment is reduced at all wind speeds by at least 18 %. The statistical values of the tower's fore-aft DELs are only marginally influenced. However, the tower side-to-side loads are increased by the LPV controller at high wind speeds. A closer analysis of the tower loads revealed that in some cases the increased pitch activity around the frequency of the lightly damped tower mode causes slightly increased tower motion. Thereby, the mean values of the DELs can increase up to 17 %. However, as the DELs on the other parts are decreased, this drawback is deemed acceptable. Further, this problem could be addressed with an integrated design of a tower damper. Further, the DELs for the pitch actuators were calculated to classify the increased pitch actuator usage. The LPV controller results in an additional increase of 35 % compared to the classical individual blade-pitch controller. This increase is comparable to that of the classical individual blade-pitch controller over the baseline-only configuration. The analyses also showed that power production is not influenced in region 3 by the proposed controller, confirming the decoupling of individual and collective blade pitch.

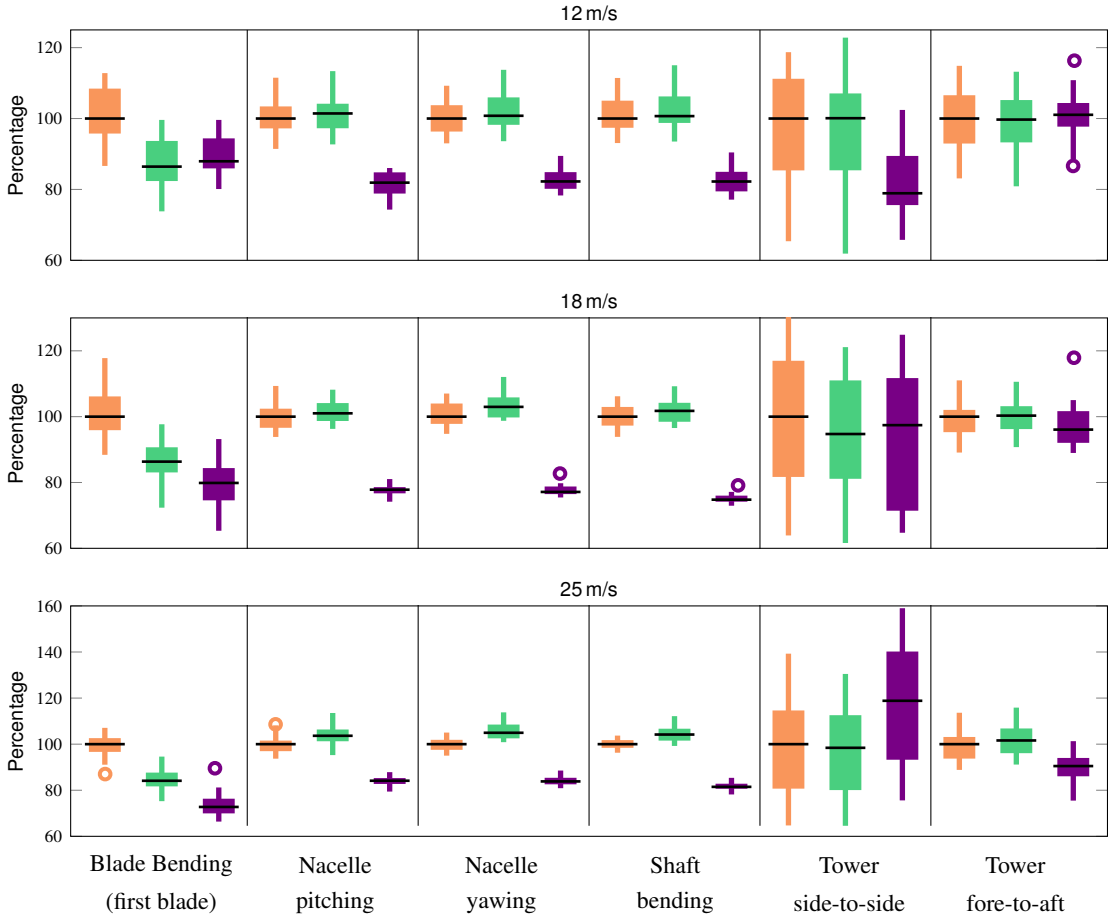

Figure 11. Statistical evaluation of loads for baseline controller ( ), two SISO integral loops ( ) and the LPV controller ( ).

6. CONCLUSION

A linear parameter-varying control design approach for an individual blade-pitch control law to reduce structural loads on the rotating and non-rotating parts of a turbine has been presented. The approach overcomes the limitation of the classical single-loops control strategy that, due to an inherent coupling at higher frequencies, can only be designed for low frequencies. Further,using the proposed approach the individual blade-pitch controller can be designed in a single design step. The proposed procedure has been successfully applied to a high-fidelity model of the utility-scale 2.5 MW research turbine operated by the University of Minnesota. Performance and stability of the wind turbine augmented with the proposed controller was verified in industry-grade nonlinear simulations.

ACKNOWLEDGEMENTS

This work was performed in the framework of the Xcel Energy Renewable Energy Fund: Contract Number RD4-13. The project title is *Virtual Wind Simulator with Advanced Control & Aeroelastic Model for Improving the Operation of Wind Farms*. This work was also supported by the National Science Foundation Grant No. NSF-CMMI-1254129 entitled *CAREER: Probabilistic Tools for High Reliability Monitoring and Control of Wind Farms*.

REFERENCES

1. Bossanyi E. Developments in closed loop controller design for wind turbines. *ASME Wind Energy Conference*, 2000; 64–74, doi:10.1002/we.34.
2. Bossanyi E. Individual Blade Pitch Control for Load Reduction. *Wind Energy* 2003; **6**(2):119–128, doi: 10.1002/we.76.
3. Coleman R, Feingold A. Theory of self-excited mechanical oscillations of helicopter rotors with hinged blades. *Technical Report*, NASA 1958.
4. Johnson W. *Helicopter Theory*. 1st edn., Princeton University Press, 1980.
5. Bir G, Wright A, Butterfield C. Stability analysis of a variable-speed wind turbine. *ASME Wind Energy Symposium*, 97-0965, 1997, doi:10.2514/6.1997-965.
6. Bossanyi E, Wright A, Fleming P. Controller field tests on the NREL CART2 turbine. *Technical Report*, National Renewable Energy Laboratory 2010.
7. Bir G. Multi-Blade Coordinate Transformation and its Application to Wind Turbine Analysis. *46th AIAA Aerospace Sciences Meeting and Exhibit*, 2008-1300, 2008, doi:10.2514/6.2008-1300.
8. Geyler M, Caselitz P. Robust Multivariable Pitch Control Design for Load Reduction on Large Wind Turbines. *Journal of Solar Energy Engineering* 2008; **130**(3), doi:10.1115/1.2931510. 031014.
9. Vali M, v Wingerden JW, Kühn M. Optimal Multivariable Individual Pitch Control for Load Reduction of Large Wind Turbines. *American Control Conference*, 2016.
10. Magar KT, Balas M, Frost S. Direct adaptive control for individual blade pitch control of wind turbines for load reduction. *Journal of Intelligent Material Systems and Structures* 2015; **12**:1564–1572, doi: 10.1177/1045389X14566527.
11. Stol KA, Zhao W, Wright AD. Individual blade pitch control for the controls advanced research turbine (CART). *Journal of Solar Energy Engineering* 2006; **128**(4):498–505, doi:10.1115/1.2349542.
12. van Engelen T. Design model and load reduction assessment for multi-rotational mode individual pitch control. *European Wind Energy Conference*, 2006.
13. Petrović V, Baotić M, Perić N. Reduction of wind turbine tower oscillations based on individual pitch control. *20th Mediterranean Conference on Control & Automation*, 2012; 1499–1505, doi:10.1109/MED.2012.6265851.
14. Bossanyi EA, Flemming P, Wright A. Validation of individual pitch control by field tests on two- and three-bladed wind turbines. *IEEE Transactions on Control Systems Technology* 2013; **21**(4):1067–1078, doi: 10.1109/TCST.2013.2258345.
15. Bossanyi E. Further Load Reductions with Individual Pitch Control. *Wind Energy* 2005; **8**(4):481–485, doi: 10.1002/we.166.
16. Barlas TK, van der Veen GJ, van Kuik GAM. Model predictive control for wind turbines with distributed active flaps: incorporating inflow signals and actuator constraints. *Wind Energy* 2012; **15**(5):757–771, doi:10.1002/we.503.
17. Unguran R, Kühn M. Combined individual pitch and trailing edge flap control for structural load alleviation of wind turbines. *American Control Conference*, 2016.
18. Larsen TJ, Madsen HA, Thomsen K. Active Load Reduction Using Individual Pitch, Based on Local Blade Flow Measurements. *Wind Energy* 2005; (8):67–80, doi:10.1002/we.14.

19. Wang N, Wright AD, Johnson KE. Independent blade pitch controller design for a three-bladed turbine using disturbance accommodating control. *American Control Conference*, 2016.
20. Wu F. Control of linear parameter varying systems. PhD Thesis, University of California, Berkley 1995.
21. EOLOS wind energy research consortium. www.eolos.umn.edu/facilities/eolos-wind-research-station.
22. Jonkman JM, Buhl ML. FAST User's Guide. *Technical Report*, National Renewable Energy Laboratory 2005.
23. Seiler P, Ozdemir A. An optimal time-invariant approximation for wind turbine dynamics using the multi-blade coordinate transformation. *American Control Conference*, 2013; 1442–1447, doi:10.1109/ACC.2013.6580039.
24. Shamma JS. Analysis and design of gain scheduled control systems. PhD Thesis, Massachusetts Institute of Technology 1988.
25. Harris M, Hand H, Wright A. LIDAR for turbine control. *Technical Report NREL/TP-500-39154*, National Renewable Energy Laboratory 2006.
26. Simley E, Pao L, Frehlich R, Jonkman B, Kelley N. Analysis of wind speed measurements using continuous wave LIDAR for wind turbine control. *49th AIAA Aerospace Sciences Meeting*, 2011, doi:10.2514/6.2011-263.
27. Lescher F, Camblong H, Curea O, Briand R. LPV control of wind turbines for fatigue loads reduction using intelligent micro sensors. *American Control Conference*, 2007; 6061–6066, doi:10.1109/ACC.2007.4282790.
28. de Corcuera AD, Pujana-Arrese A, Ezquerra JM, Milo A, Landaluze J. Linear models-based LPV modelling and control for wind turbines. *Wind Energy* 2014; **18**:1151–1168, doi:10.1002/we.1751.
29. Wu F, Yang X, Packard A, Becker G. Induced $\mathscr{L}_2$-norm control for LPV systems with bounded parameter variation rates. *International Journal of Robust and Nonlinear Control* 1996; **6**:2379–2383, doi:10.1002/(SICI)1099-1239(199611)6:9/10<983::AID-RNC263>3.0.CO;2-C.
30. Skogestad S, Postlethwaite I. *Multivariable Feedback Control – Analysis and Design*. John Wiley & Sons, 2005.
31. Zhou K, Doyle JC, Glover K. *Robust and Optimal Control*. Prentice Hall, 1996.
32. Christen U, Geering H. Inverting and noninverting $\mathscr{H}_\infty$ controllers. *Systems & Control Letters* 1997; **30**:31–38.
33. Safonov MG, Limebeer DJN, Chiang RY. Simplifying the $\mathscr{H}_\infty$ theory via loopshifting, matrix-pencil and descriptor concepts. *International Journal of Control* 1989; **50**(6):2467–2488, doi:10.1080/00207178908953510.
34. Balas G, Hjartarson A, Packard A, Seiler P. *LPVTools: A Toolbox For Modeling, Analysis, and Synthesis of Parameter Varying Control Systems* 2015. Software and User's Manual.
35. Hjartarson A, Seiler P, Packard A. LPVTools: A toolbox for modeling, analysis, and synthesis of parameter varying control systems. *1st IFAC Workshop on Linear Parameter Varying Systems*, 2015, doi: doi:10.1016/j.ifacol.2015.11.127.
36. Stein G. Respect the unstable. *IEEE Control Systems Magazine* 2003; **23**(4):12–25.
37. Blight J, Dailey RL, Gangsaas D. Practical control law design for aircraft using multivariable techniques. *International Journal of Control* 1994; **59**(1):93–137, doi:10.1080/00207179408923071.
38. Ossmann D, Theis J, Seiler P. Robust control design for load reduction on a liberty wind turbine. *ASME Dynamic Systems and Control Conference*, 2016.
39. Laino DJ, Hansen AC. USER'S GUIDE to the Wind Turbine Aerodynamics Computer Software AeroDyn. *Technical Report*, Windward Engineering, LC 2002.
40. Jonkman B, Kilcher L. TurbSim User's Guide: Version 1.50. *Technical Report NREL/TP-500-46198*, National Renewable Energy Laboratory 2009.
41. Buhl M. MCrunch Users Guide for Version 1.00. *Technical Report NREL/TP-500-43139*, National Renewable Energy Laboratory 2008.
42. Freebury G, Musial W. Determining equivalent damage loading for full-scale wind turbine blade fatigue tests. *ASME Wind Energy Symposium*, 2000-50, Reno, Nevada, USA, 2000, doi:10.2514/6.2000-50.